DOI: 10.6060/ivkkt.20196209.5945

УДК: 544.478-03

ИССЛЕДОВАНИЕ СТРУКТУРНЫХ, МИКРОСТРУКТУРНЫХ И ЭЛЕКТРОХИМИЧЕСКИХ ХАРАКТЕРИСТИК Pt/SnOx-C ЭЛЕКТРОКАТАЛИЗАТОРОВ ПОЛУЧЕННЫХ ПУТЕМ ЭЛЕКТРОХИМИЧЕСКОГО ДИСПЕРГИРОВАНИЯ ОЛОВА И ПЛАТИНЫ

А.Б. Куриганова, И.Н. Леонтьев, М.В. Авраменко, Н.В. Смирнова

Александра Борисовна Куриганова *, Нина Владимировна Смирнова

Технологический факультет, Южно-Российский государственный политехнический университет им. М.И. Платова, ул. Просвещения, 132, Новочеркасск, Российская Федерация, 346428
E-mail: kuriganova_@mail.ru*, smirnova_nv@mail.ru

Игорь Николаевич Леонтьев, Марина Владиславовна Авраменко

Физический факультет, Южный федеральный университет, ул. Зорге, 5, Ростов-на-Дону, Российская Федерация, 344090
E-mail: i.leontyev@rambler.ru, avramenko.marina@gmail.com

Порошки оксидов олова (SnO_x) с различной структурой и составом и Pt/SnO_x-C электрокатализаторы для топливных элементов с прямым окислением этанола были получены путем электрохимического диспергирования оловянных и платиновых электродов под действием импульсного переменного тока с использованием электролитов с различными типами анионов (Cl^- и F^-). Полученные порошки оксидов олова, композиционные носители SnO_x-C и катализаторы Pt/SnO_x-C были исследованы различными методами: рентгеновская дифракция, рамановская спектроскопия, сканирующая и просвечивающая электронная микроскопия. Наночастицы SnO_2 со средним размером 5 - 8 нм были синтезированы в Cl^- -содержащем растворе. В свою очередь, было обнаружено, что во F^- - содержащем электролите были получены наночастицы SnO с выраженной анизотропией формы и размером частиц. Полученные оксиды олова использовались в качестве предшественников в синтезе Pt/SnO_x-C катализаторов (загрузка Pt 20%, D_{111} = 10,5-13,5 нм) также с применением технологии электрохимического диспергирования под действием импульсного переменного тока. Электрохимически активная площадь поверхности Pt/SnO_x-C электрокатализаторов, определенная методом окислительной десорбции CO, составляла 13-15 $м^2г^{-1}$. Электрокаталитическую активность электрокатализаторов изучали для реакции электрохимического окисления этанола методами циклической вольтамперометрии с использованием вращающегося дискового электрода. Было обнаружено, что присутствие оксидов олова оказывает одинаковое влияние на реакции электрохимического окисления CO и этанола независимо от структурных особенностей их частиц.

Ключевые слова: Pt/C, оксиды олова, электроокисление этанола, электрохимическое диспергирование, топливный элемент

INVESTIGATION OF STRUCTURAL, MICROSTRUCTURAL AND ELECTROCHEMICAL CHARACTERISTICS OF Pt/SnOx-C ELECTROCATALYSTS PREPARED VIA ELECTROCHEMICAL DISPERSION OF TIN AND PLATINUM

A.B. Kuriganova, I.N. Leontyev, M.V. Avramenko, N.V. Smirnova

Alexandra B. Kuriganova, Nina V. Smirnova

Faculty of Technology, Platov South-Russian State Polytechnic University, Prosvescheniya st., 132, Novocherkassk, 346428, Russia
E-mail: kuriganova_@mail.ru*, smirnova_nv@mail.ru

Igor N. Leontyev, Marina V. Avramenko

Department of Physic, Southern University, Zorge st., 7, Rostov-on-Don, 344090, Russia
E-mail: i.leontyev@rambler.ru, avramenko.marina@gmail.com

Tin oxides powders (SnO_x) with different structure and composition and Pt/SnO_x-C electrocatalysts for the direct ethanol fuel cells have been prepared via the electrochemical dispersion of tin and platinum electrodes under a pulse alternating current using various types of anion electrolytes (Cl^- and F^- anions). As-prepared tin oxides powders, SnO_x-C composite supports and Pt/SnO_x-C catalysts have been examined by different methods: X-ray diffraction, Raman spectroscopy, scanning electron microscopy and transmission electron microscopy. SnO_2 nanoparticles with average sizes of 5 – 8 nm was prepared in a Cl^- – containing solution. In turn, the F^- – containing solution was found to contain SnO nanoparticles with pronounced shape anisotropy and diverse size of particles. These tin oxides were used as precursors in the synthesis of Pt/SnO_x-C catalysts (20% Pt loading, D_{111}=10.5 – 13.5 nm) by the same pulse alternating current technique. Electrochemical active surface area of the Pt/SnOx-C electrocatalysts determined via CO-stripping method was 13-15 m^2g^{-1}. Electrocatalytic activity of the electrocatalysts was study for the ethanol electrochemcail oxidation reaction by cyclic voltammetry, rotating disc electrode technique. It was found that the presence of tin oxides is found to exert the same promoting effect on the CO-stripping and ethanol electrochemical oxidation reaction independently on structural features of their particles.

Key words: Pt/C, tin oxides, ethanol electrooxidation, electrochemical dispersion, fuel cell

Для цитирования:
Куриганова А.Б., Леонтьев И.Н., Авраменко М.В., Смирнова Н.В. Исследование структурных, микроструктурных и электрохимических характеристик Pt/SnOx-C электрокатализаторов, полученных путем электрохимического диспергирования олова и платины. *Изв. вузов. Химия и хим. технология*. 2019. Т. 62. Вып. 9. С. 53–59

For citation:
Kuriganova A.B., Leontyev I.N., Avramenko M.V., Smirnova N.V. Investigation of structural, microstructural and electrochemical characteristics of Pt/SnOx-C electrocatalysts prepared via electrochemical dispersion of tin and platinum. *Izv. Vyssh. Uchebn. Zaved. Khim. Khim. Tekhnol*. 2019. V. 62. N 9. P. 53–59

INTRODUCTION

It is well known that the efficiency of heterogeneous catalysis processes is a result of microstructural features of the active catalytic phase - metal nanoparticles and characteristics of the support. In connection with this, the morphology of a carbon support exerts strong influence on the size of platinum particles and their distribution over the support surface [1, 2], which further impact the electronic structure, activity and selectivity of the Pt-containing catalyst [3-7].

Besides the carbon supports, there are extensively used the metal oxide supports due to high corrosion resistance, especially for catalytic processes that require the stability of the catalyst in certain temperature operating modes [8, 9]. Tin oxides are promising materials for electrocatalytic applications, especially for direct ethanol fuel cells (DEFCs) [10]. Constituting the carbon-based supports or completely replacing the carbon carriers, tin oxides serve also as co-catalysts in the anodic oxidation processes of the organic fuel, such as ethanol [11, 12].

Regarding the electrocatalytic processes, it should be noted that pure metal oxide supports remain often beyond the wide exploration because of the low conductivity of metal oxides in comparison with carbon materials. Therefore, using metal oxide-carbon composites as supports makes it possible to achieve a sought-for balance between electrical conductivity and stability of the metal oxide-carbon composites [12, 13]. It is worth noting that, depending on the metal oxide-to-carbon weight ratio, the relative powder conductivity of a composite is similar to that of carbon [12, 14].

As known, the nature of a metal oxide support in the liquid phase synthesis conditions exerts significant effect on the properties of the catalyst particles. For instance, Au particles with different sizes, formed atop a metal oxide support (TiO_2, ZnO, Al_2O_3), lead to changes in the catalytic activity [15]. The influence of particle's shape on the catalytic activity of metal oxide supports was demonstrated via the CO oxidation reaction on CeO_2-Pt hybrids with different morphologies of nano-CeO_2 (rods, cubes, and octahedra) [16]. The degree of dispersion of Pt NPs supported on Nb-doped SnO_2 aerogels and loose tubes was found to vary significantly [17]. Furthermore, SnO_2 aerogels with much smaller particle sizes exhibit the low conductivity as compared to SnO_2 loose tubes, which adversely affects the electrocatalytic properties of the Pt/SnO_2 material. Thus, a study of the influence of microstructure of the oxide support on the properties of Pr catalysts is quite mediated, revealing that the structure of oxide metal determines the platinum particle size and the degree of agglomeration of Pt nanoparticles, whereas the characteristics of platinum nanoparticles affect the electrocatalytic activity of the Pt-containing catalyst. In order to

elucidate the effect of a support itself, it is essential to use the method for catalyst synthesis that allows the catalysts to be obtained with different oxide microstructure but the same microstructure of platinum nanoparticles.

The present work aims to establish the direct influence of the tin oxide structure on the electrocatalytic properties of the Pt catalyst using the electrochemical dispersion of metals under a pulse alternating current (PAC). An important advantage of the technique based on the pulse alternating current is that metal nanoparticles, such as Pt, are formed upon the electrochemical system in a near-electrode layer and their microstructure remains independent of the nature of the support [18]. The ability to produce the dispersed tin oxides by the electrochemical oxidation and dispersion of tin electrodes in a NaCl electrolyte under the action of the alternating pulse current was earlier shown in [19]. In particular, the use of the PAC technique with different electrolytes allows one to obtain SnOx products with entirely different morphology and composition. As found, the structural peculiarities of tin oxides exert no influence on size and shape of platinum nanoparticles during their successive deposition. This method was found to be suitable for the production of both tin oxide and platinum nanoparticles, as well as for clarifying whether the structural features of SnO_x affects the electrocatalytic properties of Pt/SnO_x-C catalysts.

EXPERIMENTAL

Pt/SnO_x-C catalysts were synthesized via the pulse alternating current (PAC) procedure, as described in the [19]. At the first step, two identical tin electrodes with a geometric area of 6 cm^2 each were immersed in the aqueous solution of 1M NaCl or 1M NaF. The electrodes were connected to a PAC source, and the current density was 1 A cm^{-1}_{geom}. While exposed to the PAC, tin electrodes were oxidized and dispersed in the electrolyte. A suspension was then filtrated, washed with distillate water and dried at 80 °C to achieve a constant weight. Specimens obtained in NaCl and NaF solutions are marked below as $SnO_{x(Cl)}$ and $SnO_{x(F)}$ respectively. During the second stage, the hybrid SnO_x-C supports were prepared by mixing certain amounts of pre-synthesized tin oxides and carbon black Vulcan XC-72 in a 2M NaOH aqueous solution. The third step was aimed at obtaining Pt/SnO_x-C catalysts with respect to a technique detailed in [6]. The tin oxide loading in the catalysts was 30% and that of platinum was 20%.

Synchrotron powder diffraction (SPD) measurements were carried out at the Swiss-Norwegian Beamlines (SNBL) of the ESRF (Grénoble, France) in the Debye–Scherrer geometry at a radiation wavelength λ of 0.7121 Å using a 2-D Pilatus2M (Dectris) detector. The unit cell parameters, average crystallite size, structural microstrains and phase compositions of synthesized materials were evaluated through the Rietveld refinement on a series of symmetrized spherical harmonics for all phases in the Fullprof program [20].

The Raman spectra of samples were excited by an argon laser (λ = 514.5 nm) and recorded in the backscattering geometry over a range of 50-1000 cm^{-1} on a Renishaw spectrometer equipped with a CCD detector.

The morphology of samples was inspected in a Hitachi HT7700 transmission electron microscope. The images were acquired in the bright-field TEM mode at a 100-kV accelerating voltage.

The electrochemically active surface area (ECSA) of Pt/C and Pt/SnOx-C electrocatalysts was found by the oxidative CO_{ads} desorption (the CO stripping), as was earlier described in [12]. The EOR activity of Pt-based catalysts was measured in a 0.5 m H_2SO_4 solution by the rotating disk electrode (RDE) method in a standard three-electrode electrochemical cell. A thin catalytically active layer was deposited onto a Ø5 mm glassy carbon substrate (with a geometric area of 0.196 cm^2) and the working electrode was connected to a rotator (Pine Research Instrumentation). Electrodes were cycled between 50 to 1500 mV versus RHE while rotated at different rpms (ω = 0, 100, 225, 400, 900, 1600, and 2500 rpm).

RESULTS AND DISCUSSION

The X-ray diffraction analysis of materials prepared in both NaF and NaCl solutions showed the presence of the peaks corresponding to the tetragonal SnO phase with a space group *P*4/*nmm* and those of SnO_2 with a space group $P4_2/mnm$. In addition to these phases, the XRD pattern of $SnO_{x(Cl)}$ sample synthesized in a NaF solution exhibits the low-intensity peaks assigned to tetragonal phases $P\text{-}42_1c$ of tin(II) oxyhydroxide $Sn_6O_4(OH)_4$ [21] and β-Sn with a space group *I*4/*mmm* as well and the reflexes of the cubic-phase (*Fm*3*m)* sodium chloride. The unit cell parameters of all the above phases, the average sizes of nanoparticles, as well as the phase concentrations in samples are listed in Table 1. The data analysis in Table 1 indicates that $SnO_{x(Cl)}$ sample is almost entirely composed of SnO_2 nanoparticles whose average size is 7.6±0.5 nm.

An increase in parameters *a* and *b* and a decrease in *c* parameter in comparison with those of bulk SnO_2 (ICSD database no. 154960) are likely due to size effects [22]. In turn, the $SnO_{x(F)}$ sample possess the predominance of SnO.

Table 1

Lattice parameter and average particle size calculated through the Rietveld refinement

***Таблица 1.* Параметры решетки и средний размер частиц, рассчитанные по методу Ритвельда**

Sample	Space group	Unit cell parameter, Å	D_{av}, nm*	Concentration, %
$SnO_{x(Cl)}$	SnO (*P*4/*nmm*)	*a* = *b* = 3.789(8) *c* = 4.824(4)	71.0±0.5	~3
	SnO_2 ($P4_2/mnm$)	*a* = *b* = 4.738(6) *c* = 3.171(7)	7.6±0.5	96
	NaCl (*Fm3m*)	-	-	<1
$SnO_{x(F)}$	SnO (*P*4/*nmm*)	*a* = *b* = 3.799(8) *c* = 4.839(6)	-	~85
	SnO_2 ($P4_2/mnm$)	*a* = *b* = 4.749(6) *c* = 3.171(9)	5.5±0.5	~12
	Sn (*41/amd*)	*a* = *b* = 5.829(3) *c*=3.176(6)Å	-	~2
	$Sn_6O_4(OH)_4$ ($P\text{-}42_1c$)	*a* = *b* = 7.9268(4) *c* = 9.1025(5)	-	~1

Note: * The dashed line in the graph of the average particles size indicates the impossibility of accurately determining the average particle size from XRD data (the diffraction peak width of the phases does not exceed the width corresponding to the instrumental broadening function)

Примечание: * Пунктирная линия на графике среднего размера частиц указывает на невозможность точного определения среднего размера частиц по данным РФА (ширина дифракционного пика фаз не превышает ширину, соответствующую инструментальной функции уширения)

The interpretation of Raman spectra of samples is given in Table 2. A variety of bands emerges in a range of 50-800 cm^{-1}, where ten of them are attributed to tetragonal SnO_2 (including five disorder-induced IR-modes), two are assigned to SnO, and the rest of the modes are those induced by the doping of SnO_x ($1 < x < 2$) nanoparticles with halogen (Cl for $SnO_{x(Cl)}$/F for $SnO_{x(F)}$) atoms [23]. Unlike the XRD results, the Raman spectrum of $SnO_{x(Cl)}$ sample exhibits no vibrations of NaCl due to the fact that the first-order Raman spectrum of NaCl is forbidden and the second-order one is hardly detectable [30]. Since the total area ratio of disorder-induced modes to that of A_{1g} of tetragonal SnO_2 for both samples is about 4, it can be concluded that the average diameter of SnO_2 nanoparticles is about 5-10 nm that is consistent with XRD data.

Table 2

Summary of Raman data acquired

***Таблица 2.* Результаты исследований методом комбинационного рассеяния света**

Raman shift in $SnO_{x(Cl)}$ / $SnO_{x(F)}$ sample, cm^{-1}	Interpretation	
	Tin-oxide phase	Modes description
64 / 61	Halogen (Cl / F)-doped SnO_x ($1<x<2$)	The modes induced by the doping of SnO_x ($1<x<2$) nanoparticles with halogen (Cl / F) atoms
- / 71		
79 / 82		
94 / 97		
- / 102		
110 / 109	SnO	B_{1g}
- / 120	Halogen (Cl / F)-doped SnO_x ($1<x<2$)	The modes induced by the doping of SnO_x ($1<x<2$) nanoparticles with halogen (Cl / F) atoms
135 / 137		
167 / 164		
- / 181		
208 / 206	SnO	A_{1g}
247 / 248	SnO_2	disorder-induced IR-mode E_u
305 / 300		disorder-induced IR-mode E_u
344 / 346		surface mode B_1
469 / 464		E_g
493 / 496		disorder-induced IR-mode A_{2u}
561 / 563		surface mode B_2
624 / 623		A_{1g}
685 / 683		disorder-induced IR-mode A_{2u}
740 / 740		disorder-induced IR-mode E_u
770 / 771		B_{2g}

Fig. 1 displays the SEM and TEM images of tin oxides prepared during the first step. A sample of $SnOx_{(Cl)}$ obtained in a NaCl electrolyte is composed of spherical particles with sizes of 5-8 nm. $SnOx_{(F)}$ samples synthesized in a NaF solution are characterized by a strong anisotropy of shape and diverse size of the particles. Furthermore, two different phases of this sample can be distinguished that are spherical structures with a nanometric size and macrometric nanosheets consisting of agglomerated nanoparticles, as coincides with XRD data revealing the presence of two phases as well.

The Pt catalysts based on $SnO_{x(F)}$–C and $SnO_{x(Cl)}$–C hybrid supports were also probed via XRD. The XRD patterns of Pt/C prepared using the same way [18], as well as those of Pt/$SnO_{x(F)}$–C and Pt/$SnO_{x(Cl)}$–C catalysts synthesized by the pulse alternating current technique, are shown in Fig. 2. Three well-resolved diffraction peaks at 39.6, 46.1 and 67.5 are assigned to (111), (200) and (220) crystal planes of a Pt face-cen-

tered cubic structure [space group Fm3m (no. 225) respectively. In fact, the particle size D_{111} along the (111) direction, calculated from the Scherrer equation, is 10.5-13.5 nm. The diffraction peaks attributed to the tin oxides exhibit the lower intensities.

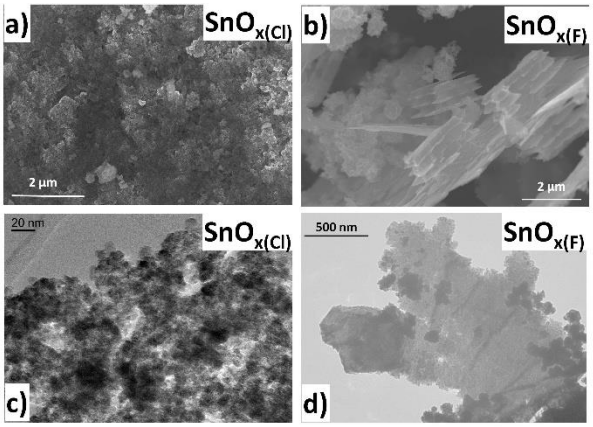

Fig. 1. SEM (a, b) and TEM (c, d) images of SnO_x(Cl) and SnO_x(F) samples
Рис. 1. СЭМ (a, b) и ПЭМ (c, d) изображения образцов SnO_x(Cl) и SnO_x(F)

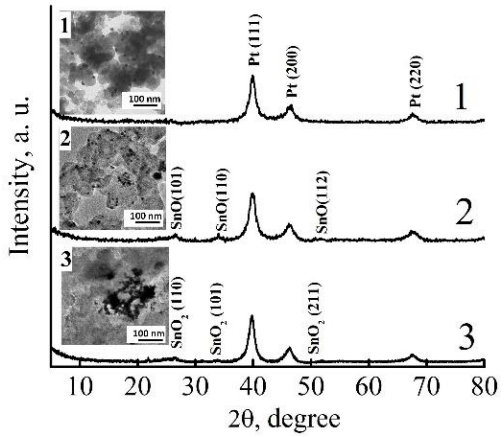

Fig. 2. XRD-patterns and TEM images of Pt/C – 1, Pt/SnO_x (Cl)-C – 2 and Pt/SnO_x(F)-C – 3 catalysts obtained via the PAC method
Рис. 2. Рентгенограммы и ПЭМ изображения Pt/C – 1, Pt/SnO_x (Cl)-C – 2 и Pt/SnO_x(F)-C – 3 катализаторов, полученных методом электрохимического диспергирования

The electrochemically active surface areas (ECSAs) of catalysts, measured via the CO-stripping, are listed in Table 3. The largest ECSA is found for the Pt/$SnO_{x(F)}$-C catalyst, which may be due to the lower degree of Pt particle agglomeration in comparison with Pt/C and Pt/$SnOx_{(Cl)}$-C nanocomposites (Fig. 2). Moreover, the onset CO oxidation potentials on the catalysts based on $SnO_{x(F)}$-C and $SnO_{x(Cl)}$-C hybrid supports are shifted in the cathodic direction, i.e. the overvoltage oxidation of CO adsorbed on platinum decreases (see Fig. 3 and Table 3).

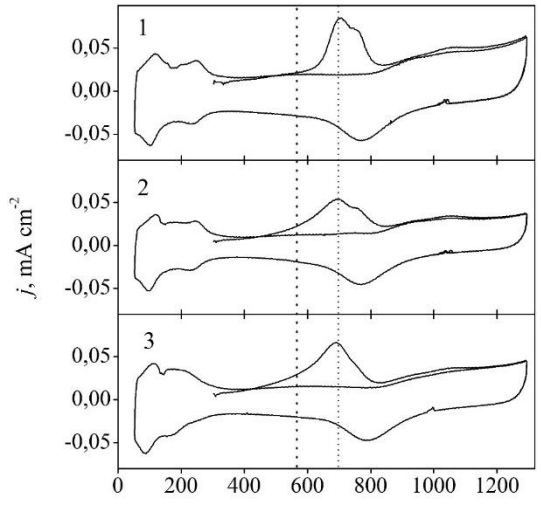

Fig. 3. CO-stripping of Pt/C – 1, Pt/SnO_x(Cl)-C – 2, Pt/SnO_x(F)-C – 3 catalysts in 0.5M H_2SO_4, the scan rate is 20 mV s^{-1}
Рис. 3. Электрохимическое окисления CO на Pt/C – 1, Pt/SnO_x(Cl)-C – 2, Pt/SnO_x(F)-C – 3 катализаторах в 0,5М H_2SO_4, скорость развертки потенциала 20 мВ $с^{-1}$

Table 3

Electrochemical characteristics of Pt-based catalysts obtained via the PAC technique

***Таблица 3.* Электрохимические характеристики катализаторов на основе Pt, полученных методом электрохимического диспергирования**

Sample	CO-striping		EOR	
	E_{onset}, mV	ECSA, $m^2 \cdot g^{-1}$	E_{onset}, mV	$SA_{0.6V}$, $mA \cdot cm^{-2}$
Pt/C	516	13.1±1.3	500	0.063
Pt/$SnO_{x(F)}$-C	458	15.2±1.5	495	0.065
Pt/$SnO_{x(Cl)}$-C	427	13.5±1.2	480	0.114

Fig. 4 displays the cyclic voltammetry curves acquired on Pt/C in a 0.5 M H_2SO_4 + 0.5 M EtOH solution. Three distinct features of the oxidation current are attributed to the EOR: the first one between E = 0.4 and E = 1.0 V vs. RHE, a second one at E > 1.1 V vs. RHE (both in the anodic scan), and the last one located between E = 0.8 and 0.4 V vs. RHE during the cathodic scan. The non-linear dependence of the current density of ethanol oxidation peaks on the disk rotation speed was established on the forward scan of the CV-curve in a potential range of 0.4-1.0 V vs RHE (Fig. 4), indicating the complexity of the EOR reaction. In addition, the nonlinear dependence means that the reaction rate in this case remains independent of the reagent access to the catalyst surface, but also of the formation/desorption/poisoning by adsorbed particles of the platinum surface [24]. The rise in the ethanol electrooxidation rate and the overpotential lose during this process are due to the bifunctional mechanism of ethanol electrooxidation on platinum in the presence of SnO_2. The

enhanced electrocatalytic activity of Pt/SnO_x-C catalysts toward the EOR in comparison with Pt/C is therefore brought by the bifunctional mechanism (equation 1-5) in which the activated water from SnO_x at low potentials (equation 2, 3) promotes the oxidative removal of the intermediates of ethanol electrooxidation from Pt sites (equation 4, 5) [25]. The strong interactions between H_2O and SnO_x surfaces can lead to spontaneous breakage of one of the O–H bonds [26].

Despite the fact that the surface activity of Pt/SnO_x-C catalysts exceeds that of Pt/C, as is observed from the current density of the ethanol oxidation peaks in the forward and reverse scans of the CV-curves and at a potential of 0.6 V (Fig. 4, Table 3).

$$Pt + CO \rightarrow Pt–CO_{ad} \quad (1)$$

$$Sn + H_2O \rightarrow Sn–OH_{ad} + H^+ + e^- \quad (2)$$

$$SnO_x + H_2O \rightarrow SnO_x–OH_{ad} + H^+ + e^- \quad (3)$$

$$Pt–CO_{ad} + Sn–OH_{ad} \rightarrow CO_2 + H^+ + e^- \quad (4)$$

$$Pt–CO_{ad} + SnO_2–OH_{ad} \rightarrow CO_2 + H^+ + e^- \quad 5)$$

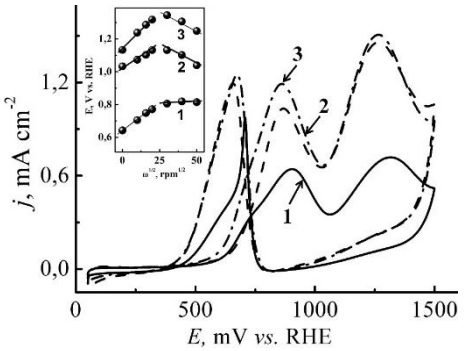

Fig. 4. CV curves of Pt/C – 1, Pt/SnO_x(F)-C – 2, Pt/SnO_x(Cl)-C – 3 in 0.5M EtOH + 0.5 M H2SO4 , 50 mV s^{-1} and rotation speed dependences of anodic peak current densities

Рис. 4. ЦВА Pt/C – 1, Pt/SnO_x(F)-C – 2, Pt/SnO_x(Cl)-C – 3 катализаторов в 0,5M EtOH + 0,5 M H_2SO_4, скорость развертки потенциала 50 мВ/с и зависимости плотностей тока пика на анодном ходе кривой от скорости вращения

In this respect, neither the composition nor the structural characteristics of SnO_x particles prepared via the PAC method is the parameter defining the electrocatalytic properties of Pt-containing catalysts. This is most likely to be due to the fact that the surface of SnO is always coated with a SnO_2 layer, and the interactions between H_2O and SnO_x surfaces do not depend on the tin oxide particle size, which is a key factor determining the high rate of ethanol oxidation on Pt/SnO_x-C catalytic systems in comparison with Pt/C.

CONCLUSIONS

Tin oxides with different microstructure and composition were synthesized in NaCl and NaF solutions via the pulse alternating current method. A comprehensive analysis of samples using XRD, Raman spectroscopy, TEM, and SEM revealed the formation of SnO_2 nanoparticles with average sizes of 5-8 nm in a NaCl solution. In turn, the NaF solution was found to contain SnO nanoparticles with pronounced shape anisotropy and diverse size of particles. These tin oxides were used as precursors in the synthesis of Pt/SnOx-C catalysts (20% Pt loading, D_{111} = 10.5-13.5 nm) by the same pulse alternating current technique. The electrocatalytic properties of produced catalysts were studied towards the CO-stripping and the ethanol electrooxidation reaction. The results revealed a promotion effect of tin oxides on both Pt/SnOx-C catalysts independently of their structural features.

XRD, Raman spectroscopy, TEM measurements were carried out with the financial support by the Russian Science Foundation (Grant No. 14-23-00078).

All electrochemical measurements were carried out with the financial support by the Grant from the President of the Russian Federation for young Ph.D. scientists MK-194.2019.3.

REFERENCES
ЛИТЕРАТУРА

1. **Tuaev X., Rudi S., Strasser P.** The impact of the morphology of the carbon support on the activity and stability of nanoparticle fuel cell catalysts. *Catal. Sci. Technol*. 2016. V. 6. P. 8276-8288. DOI: 10.1039/C6CY01679K.
2. **Kulbakov A.A., Kuriganova A.B., Allix M., Rakhmatullin A., Smirnova N., Maslova O.A., Leontyev I.N.** Non-isothermal decomposition of platinum acetylacetonate as a cost-efficient and Size-Controlled Synthesis of Pt/C nanoparticles. *Catal. Commun*. 2018. V. 117. P. 14-18. DOI: 10.1016/j.catcom.2018.08.022.
3. **Xia X., Yates J.L.R., Jones G., Sarwar M., Harkness I., Thompsett D.** Theoretical exploration of novel catalyst support materials for fuel cell applications. *J. Mater. Chem. A*. 2016. V. 4. P. 15181-15188. DOI: 10.1039/C6TA05399H.
4. **Shi Y., Li X., Rong X., Gu B., Wei H., Sun C.** Influence of support on the catalytic properties of Pt-Sn-K/[small theta]-Al_2O_3 for propane dehydrogenation. *RSC Adv*. 2017. V. 7. P. 19841-19848. DOI: 10.1039/C7RA02141K.
5. **Sevjidsuren G., Zils S., Kaserer S., Wolz A., Ettingshausen F., Dixon D., Schoekel A., Roth C., Altantsog P., Sangaa D., Ganzorig C.** Effect of Different Support Morphologies and Pt Particle Sizes in Electrocatalysts for Fuel Cell Applications. *J. Nanomaterials*. 2010. V. 2010. P. 1-9. DOI: 10.1155/2010/852786.
6. **Novikova K., Kuriganova A., Leontyev I., Gerasimova E., Maslova O., Rakhmatullin A., Smirnova N., Dobrovolsky Y.** Influence of Carbon Support on Catalytic Layer Performance of Proton Exchange Membrane Fuel Cells. *Electrocatal*. 2018. V. 9. P. 22-30. DOI: 10.1007/s12678-017-0416-4.
7. **Koningsberger D.C., Ramaker D.E., Miller J.T., de Graaf J., Mojet B.L.** The direct influence of the support on the electronic structure of the active sites in supported metal catalysts: evidence from Pt–H anti-bonding shape resonance and Pt–CO FTIR data. *Top. Catal.* 2001. V. 15. P. 35-42. DOI: 10.1023/a:1009067712537.

8. **Monyoncho E.A., Ntais S., Brazeau N., Wu J.-J., Sun C.-L., Baranova E.A.** Role of the Metal-Oxide Support in the Catalytic Activity of Pd Nanoparticles for Ethanol Electrooxidation in Alkaline Media. *Chem. Elect. Chem.* 2016. V. 3. P. 218-227. DOI: 10.1002/celc.201500432.
9. **Seth J., Dubey P., Chaudhari V.R., Prasad B.L.V.** Preparation of metal oxide supported catalysts and their utilization for understanding the effect of a support on the catalytic activity. *New J. Chem.* 2018. V. 42. P. 402-410. DOI: 10.1039/C7NJ03753H.
10. **James D.D., Moghaddam R.B., Chen B., Pickup P.G.** Ruthenium-Tin Oxide/Carbon Supported Platinum Catalysts for Electrochemical Oxidation of Ethanol in Direct Ethanol Fuel Cells. *J. Electrochem. Soc.* 2018. V. 165. P. F215-F219. DOI: 10.1149/2.1071803jes.
11. **Antolini E.** Catalysts for direct ethanol fuel cells. *J. Power Sour.* 2007. V. 170. P. 1-12. DOI: 10.1016/j.jpowsour.2007.04.009.
12. **Kuriganova A.B., Leontyeva D.V., Ivanov S., Bund A., Smirnova N.V.** Electrochemical dispersion technique for preparation of hybrid MO x –C supports and Pt/MOx–C electrocatalysts for low-temperature fuel cells. *J. Appl. Electrochem*. 2016. V. 46. P. 1245-1260. DOI: 10.1007/s10800-016-1006-5.
13. **Luo Y., Alonso-Vante N.** The Effect of Support on Advanced Pt-based Cathodes towards the Oxygen Reduction Reaction. State of the Art. *Electrochim. Acta*. 2015. V. 179. P. 108-118. DOI: 10.1016/j.electacta.2015.04.098.
14. **Ma J., Habrioux A., Alonso-Vante N.** The Effect of Substrates at Cathodes in Low-temperature Fuel Cells. *Chem. Electr. Chem.* 2014. V. 1. P. 37-46. DOI: 10.1002/celc.201300105.
15. **Ousmane M., Liotta L.F., Pantaleo G., Venezia A.M., Di Carlo G., Aouine M., Retailleau L., Giroir-Fendler A.** Supported Au catalysts for propene total oxidation: Study of support morphology and gold particle size effects. *Catal. Today*. 2011. V. 176. P. 7-13. DOI: 10.1016/j.cattod.2011.07.009.
16. **Singhania N., Anumol E.A., Ravishankar N., Madras G.** Influence of CeO_2 morphology on the catalytic activity of CeO_2-Pt hybrids for CO oxidation. *Dalton transact*. 2003. V. 42. P. 15343-15354. DOI: 10.1039/c3dt51364e.
17. **Cognard G., Ozouf G., Beauger C., Jiménez-Morales I., Cavaliere S., Jones D., Rozière J., Chatenet M., Maillard F.** Pt Nanoparticles Supported on Niobium-Doped Tin Dioxide: Impact of the Support Morphology on Pt Utilization and Electrocatalytic Activity. *Electrocatal*. 2017. V. 8. P. 51-58. DOI: 10.1007/s12678-016-0340-z.
18. **Leontyev I., Kuriganova A., Kudryavtsev Y., Dkhil B., Smirnova N.** New life of a forgotten method: Electrochemical route toward highly efficient Pt/C catalysts for low-temperature fuel cells. *Appl. Catal. A: Gen*. 2012. V. 431. P. 120-125. DOI: 10.1016/j.apcata.2012.04.025.
19. **Kuriganova A.B., Vlaic C.A., Ivanov S., Leontyeva D.V., Bund A., Smirnova N.V.** Electrochemical dispersion method for the synthesis of SnO2 as anode material for lithium ion batteries. *J. Appl. Electrochem.* 2016. V. 46. P. 527-538. DOI: 10.1007/s10800-016-0936-2.
20. **Carvajal J.** FULLPROF: A Program for Rietveld Refinement and Pattern Matching Analysis. Abstracts of the Satellite Meeting on Powder Diffraction of the XV Congress of the IUCr. 1990. Citeulike-article-id:1840305.
21. **Abrahams I., Grimes S.M., Johnston S.R., Knowles J.C.** Tin(II) Oxyhydroxide by X-ray Powder Diffraction. *Acta Cryst. C.* 1996. V. 52. P. 286-288. DOI: 10.1107/S0108270195012625.
22. **Diehm P.M., Agoston P., Albe K.** Size-dependent lattice expansion in nanoparticles: reality or anomaly? *Chemphyschem: Eur. J. chem. Phys. Phys. Chem.* 2012. V. 13. P. 2443-2454. DOI: 10.1002/cphc.201200257.
23. **Noor N., Parkin I.P.** Enhanced transparent-conducting fluorine-doped tin oxide films formed by Aerosol-Assisted Chemical Vapour Deposition. *J. Mater. Chem. C.* 2013. V. 1. P. 984-996. DOI: 10.1039/C2TC00400C.
24. **Bach Delpeuch A., Jacquot M., Chatenet M., Cremers C.** The influence of mass-transport conditions on the ethanol oxidation reaction (EOR) mechanism of Pt/C electrocatalysts. *PCCP*. 2016. V. 18. P. 25169-25175. DOI: 10.1039/C6CP04294E.
25. **Moghaddam R.B., Pickup P.G.** Support effects on the oxidation of ethanol at Pt nanoparticles. *Electrochim. Acta*. 2012. V. 65. P. 210-215. DOI: 10.1016/j.electacta.2012.01.042.
26. **Zhou W.-P., Axnanda S., White M.G., Adzic R.R., Hrbek J.** Enhancement in Ethanol Electrooxidation by SnOx Nanoislands Grown on Pt(111): Effect of Metal Oxide–Metal Interface Sites. *J. Phys. Chem. C.* 2011. V. 115. P. 16467-16473. DOI: 10.1021/jp203770x.

Поступила в редакцию 20.12.2018
Принята к опубликованию 11.07.2019

Received 20.12.2018
Accepted 11.07.2019